FISEVIER

Contents lists available at ScienceDirect

Journal of Alloys and Compounds

journal homepage: www.elsevier.com/locate/jalcom



Research Article

Strongly luminescent and highly stable CsPbBr₃/Cs₄PbBr₆ core/shell nanocrystals and their ultrafast carrier dynamics



Chenxu Wang, Lihe Yan *, Jinhai Si, Tianyu Huo, Xun Hou

Key Laboratory for Physical Electronics and Devices of the Ministry of Education and Shaanxi Key Laboratory of Photonics Technology for Information, School of Electronic Science and Engineering, Xi'an Jiaotong University, No.28, Xianning West Road, Xi'an 710049, China

ARTICLE INFO

Article history:
Received 12 December 2022
Received in revised form 8 February 2023
Accepted 11 February 2023
Available online 13 February 2023

Keywords:
Perovskite nanocrystal
Core/shell nanostructure
Heterojunction
Carrier dynamics

ABSTRACT

All-inorganic lead halide perovskites nanocrystals (NCs) have been demonstrated to be promising candidates for optoelectronic devices, but preparing perovskite NCs with high photoluminescence quantum yields (PLQYs) and excellent stability has been a challenge. In this work, CsPbBr₃/Cs₄PbBr₆ core/shell NCs with a PLQYs of 87.23% and long-term stability in ambient environments was prepared by room temperature inverse microemulsion method. The excellent stability of the sample was attributed to the protection of Cs₄PbBr₆, and higher PLQYs could be owing to the passivation effect of the core/shell structure. To illustrate the distribution of photogenerated carrier in the core/shell structure, a confined excitons model was proposed based on time-resolved PL and temperature dependent PL measurements. Femtosecond time-resolved transient absorption spectra measurements were performed upon different excitation wavelength to unveil the photogenerated carrier dynamics in core/shell NCs. Upon 300 nm excitation, a carrier transfer process with the time of 3.18 ps from shell to core layer was observed. Furthermore, both two- and three-photon absorption PL was discovered in core/shell NCs, further verifying the carrier transfer process.

© 2023 Elsevier B.V. All rights reserved.

1. Introduction

Over the last decade, colloidal all-inorganic lead halide perovskite nanocrystals (CsPbX₃ NCs, X = Cl, Br and I) have rapidly emerged as one of the most promising materials of optoelectronic devices [1–4], benefiting from their unique properties, such as the high photoluminescence quantum yields (PLQYs), tunable emission wavelength and narrow emission bandwidth. The defects of perovskite are dominated by shallow defect state energy levels and exhibit excellent defect tolerance [5], resulting in a higher proportion of radiative recombination. Compared with traditional group III-V nanocrystals [6], CsPbX₃ NCs have exhibited higher PLQYs (> 50%), making it a prospecting luminescent material for illumination and display [7].

Despite these advantages, poor stability still limits the commercial applications of lead halide perovskite nanocrystals. Perovskite NCs would show a rapid decline in luminescence properties when suffer from chemical, light or thermal due to the "soft" ionic structure [8–10]. It has been pointed out that in humid environments, nanocrystals would degrade when irradiated by ultraviolet (UV) [9],

* Corresponding author. E-mail address: liheyan@mail.xjtu.edu.cn (L. Yan). making it a challenge for displays. For dealing with these issues, various strategies such as surface passivation [11,12], doping [13,14], and encapsulation [15,16] have been proposed. Especially, introducing suitable encapsulation can not only prevent the invading of water and oxygen, but also effectively improve the utilization efficiency of photogenerated carriers in CsPbX₃ NCs promoting the PLQYs. Until now, kinds of materials like SiO₂ [17], Al₂O₃ [18], PbSO₄ [19], ZnS [20], TiO₂ [21], CdS [22,23] have been applied as the protective layer of CsPbBr₃ NCs.

Besides the stability, reducing surface state defects and further promoting the PLQYs is another point for the applications of CsPbX₃ NCs [24]. Although the stability of CsPbBr₃ NCs could be improved by encapsulation, lattice mismatch between the heterogeneous packaging materials and CsPbX₃, which would deteriorate their luminescence performance, is nonnegligible [25]. Cs₄PbBr₆, often called "zero-dimensional (0D) perovskites" as the PbX₆⁴⁻ octahedra is no longer corner-shared compared with corner-sharing PbX₆⁴⁻ octahedra in CsPbBr₃, has been proposed as a coating material in recent years [25–28]. Isolated PbX₆⁴⁻ octahedra separated from each other by a Cs⁺ ion inserted in the crystal lattice is beneficial in maintaining the structure of Cs₄PbBr₆, exhibiting excellent thermal and anion exchange stability [29]. Relevant studies have shown that in conventional environments, Cs₄PbBr₆ exhibited better environmental tolerance than CsPbBr₃ [30]. Significantly, Cs₄PbBr₆ lattice spacing

matches well with the CsPbBr₃ lattice [25], which can enhance the surface passivation without additional strain on the NCs. Besides, due to the same constituent elements for CsPbBr₃ and Cs₄PbBr₆, elemental doping can be avoided [31]. Jia et al. [32] reported the CsPbBr₃/Cs₄PbBr₆ core shell structure for the first time, with improved stability and PLQYs. Then, Ge et al. [31], Chen et al. [33] also prepared the CsPbBr₃/Cs₄PbBr₆ core/shell materials and demonstrated their applications in heat-resistant fluorescent inks and phosphors. Nevertheless, the preparations of core/shell structure in the previous reports were usually accompanied by harsh synthesis conditions and complicated steps, and PLQYs enhancement mechanism as well as photogenerated carrier transfer dynamics in the core/shell structure are still lack of the systematic illustrations.

In this work, a facile room temperature inverse microemulsion method was adopted to produce CsPbBr₃ NCs and CsPbBr₃/Cs₄PbBr₆ core/shell NCs by changing the precursor ratio of cesium source and lead source. Compared with the CsPbBr₃ NCs, the CsPbBr₃/Cs₄PbBr₆ core/shell NCs exhibited an excellent photophysical property with an improved PLQYs from 45% to 87.23% after shell coating. The core/ shell NCs showed remarkable stability under conventional atmospheric environment. We conclude that the Cs₄PbBr₆ shell could not only lead to the surface defects passivation of CsPbBr3 NCs, but also form a typical quantum well structure due to its wide bandgap structure (4.0 eV), which could bind the photogenerated electronhole in the CsPbBr₃ (2.4 eV) NCs and further enhance the electronhole radiation recombination. The speculations were confirmed by various kinds of characterization including UV-Visible absorption spectroscopy (UV-Vis), photoluminescence spectroscopy (PL), timeresolved fluorescence spectroscopy (TRPL), time-resolved transient absorption spectroscopy and multi-photon absorption spectroscopy. The intrinsic photophysical mechanism was revealed, and a confined excitons model was put forward to illustrate the carrier transfer process in CsPbBr₃/Cs₄PbBr₆ core/shell NCs.

2. Experimental section

2.1. Materials

Cesium carbonate (Cs_2CO_3 , Aldrich, 99.9% metals basis), Lead (II) bromide (PbBr₂, Meryer, 99%), Oleic acid (OA, Meryer, 85%), Oleylamine (OAm, Meryer, C18: 80–90%), Hexane (C_6H_{14} , Sinopharm Chemical Reagent Co., Ltd, \geq 97.0%), N, N-dimethylformamide (DMF, Aladdin, \geq 99.9% (GC)), Hydrobromic acid (HBr, 48 wt% in H_2O , Macklin, ACS).

2.2. Synthesis of Cs-oleate precursor

1.125 g Cs_2CO_3 and 10.75 mL OA were taken in 50 mL 3-necked round bottom flask and the mixture was kept in vacuum for 20 mins followed by purging with N_2 for 20 mins along at 100 °C by Schlenk system with continuously magnetic stirring. The process of alternate application of vacuum and N_2 was repeated for 3 times to remove the moisture and O_2 in the reaction mixture. The temperature of the reaction mixture was then increased to 150 °C, and continued until the Cs_2CO_3 reacted and turned to a yellowish stock of Cs-oleate precursor, and then stored in a vial for further processing.

2.3. Synthesis of CsPbBr₃ NCs

Typically, perovskite nanocrystals were synthesized using a facile reverse microe-mulsion method. $50 \mu L$ Cs-oleate precursor, 10 mL nhexane, 5 mL OA were mixed in a 20-mL glass vial for 10 min mild stirring at a $35 \,^{\circ}\text{C}$ heating plate to eliminate the influence of ambient temperature changes. To avoid the influence of moisture and O_2 on the reaction, OA was degassed at $100 \,^{\circ}\text{C}$ by Schlenk system. Meanwhile, 1 mL PbBr₂ (0.03 M, DMF), $2 \mu L$ HBr (48%), 0.1 mL OA,

and 0.05 mL OAm were loaded in a 2-mL glass vial for 10 min mild stirring. Subsequently, the latter was dropped into the former under vigorous stirring. The color changes from colorless to green with the addition of lead precursors. 10 mins later, the as-synthesized nanocrystals were collected via centrifugation at 8000 rpm for 3 min, followed by dispersion in 4 mL of hexane for further characterization.

2.4. Synthesis of CsPbBr₃/Cs₄PbBr₆ core/shell NCs

Similar to the specific experimental steps of CsPbBr₃ NCs, by adjusting the precursor ratio of lead to cesium, CsPbBr₃ /Cs₄PbBr₆ core/shell NCs was synthesized. In addition to what 100 μ L Cs-oleate precursor was applied for cesium-rich solution and 15 μ L HBr (48%) instead of 2 μ L HBr (48%), for PbBr₂ solution are all the same.

2.5. Characterization

Powder X-ray diffraction was performed using a Shimadzu XRD-6100 diffractometer with Cu-K α radiation (λ = 1.5406 Å). The samples were prepared via the drop casting of the nanocrystal suspension onto a clean glass slide, followed by drying at room temperature (For the temperature-dependent photoluminescence spectra below, the same sample preparation method was used.). A UV-2600 spectrophotometer (Shimadzu) was employed to examine the absorption spectra. The photoluminescence spectra were recorded by OmniFluo960 spectrometer (Zolix). Time-resolved PL spectra, PLQYs and temperature-dependent photoluminescence spectra were recorded using FLS920 spectrometer (Edinburgh). For time-resolved PL spectra, a picosecond pulsed LED (central wavelength: 450 nm, repetition rate: 10 MHz) was used as the excitation light source. For PLQYs and temperature-dependent photoluminescence spectra, excitation light source (410 nm) was selected from Xe lamp spectrum. Transmitted electron microscopy (TEM) images and high resolution TEM (HRTEM) images were acquired by the Talos F200X Lorenz transmission electron microscope with an acceleration voltage of 200 keV, to which an Oxford energy dispersive X-ray spectroscopy (EDX) system X-max50 was coupled for EDX-SEM mapping analysis.

2.6. Femtosecond time-resolved transient absorption

Femtosecond time-resolved transient absorption (TA) measurements were employed on a home-built setup with pump and probe beams generated by a mode locked amplified Ti: sapphire laser system (Coherent Legend, 800 nm, 150 fs, and 1 kHz repetition rate). The 400 nm pump beam was operated at second harmonic generation (SHG) of 800 nm beam. The probe beam, white light continuum (WLC) ranging from 450 to 750 nm, was produced by focusing the 800 nm pulses into a 1-mm-thick sapphire plate. A motorized delay stage was applied to control the delay between the pump and probe pulses. The repetition rate of pump beam was reduced to 500 Hz using a synchronized chopper. The transmitted probe pulses from the samples were collected by a fiber-coupled spectrometer. By comparing the transmitted probe pulses with and without pump pulse, TA spectra as a function of the delay time between the pump and probe pulses were obtained. In the measurements, all samples were filled in 1 mm cuvettes.

In the TA measurements, TA signal intensity was characterized using optical density expressed by $A_x = \log (I_0/I)$, where I is the transmitted probe light intensity and I_0 is the incident probe light intensity. The time dependent light-induced absorption change caused by the pump pulse could be evaluated by the difference between probe light intensity measured with (I_{pump}) and without (I_{unpump}) the pump pulse, which was calculated using the following formula.

$$\Delta A(\lambda,t) = \log \left(\frac{I_0}{I_{pump}}\right) - \log \left(\frac{I_0}{I_{umpump}}\right)$$

$$= \log(\frac{I_{umpump}}{I_{pump}})$$

where t is the delay time between the pump and probe pulses and λ is the wavelength of the probe light. Ground state bleaching and excited state absorption are two typical TA signals. When the sample is excited, electrons in the ground state are excited to the excited state, and the ground state absorption would be weakened, causing the ground state bleaching and leading to negative TA signals in the region near the wavelength of the ground state absorption. The material in the excited state could also further absorb the probe light and transition to the excited state of higher energy level. This will induce the excited state absorption, leading to a positive signal in the TA spectra. Besides, stimulated emission effects could take place in some luminescent materials, which could cause the enhancement of the probe light, inducing a negative TA signal.

2.7. Two- and multi-photon absorption PL measurements

Two- and multi-photon absorption PL measurements were conducted on a home-built platform using 800 nm femtosecond laser. Femtosecond laser was focused into the NCs samples by a lens with a focal length of 20 cm. Two continuously variable neutral density filters were employed to control the incident energy of the laser pulses, and the PL emissions from the samples were collected by a lens and recorded by a spectrometer.

3. Results and discussion

CsPbBr₃ NCs and CsPbBr₃/Cs₄PbBr₆ core/shell NCs were synthesized via a facile inverse microemulsion method, with detailed processes presented in Experimental section. Concise preparation processes and corresponding schematic diagram of the core-shell structure are shown in Fig. 1a and 1b, respectively. Two precursors were mixed for 10 min and CsPbBr₃ NCs and CsPbBr₃/Cs₄PbBr₆ core/ shell NCs were prepared by changing the proportion of lead and cesium precursors, respectively. As shown in Fig. 1c, CsPbBr₃ NCs yielded a typical absorption edge at a wavelength of 510 nm and PL peaked at 514 nm. For CsPbBr₃/Cs₄PbBr₆ core/shell NCs, however, an additional absorption peak was observed at 313 nm, corresponding to the absorption peak of Cs₄PbBr₆. Except for the absorption peak at 313 nm, both the absorption edge (505 nm) and PL peak position (510 nm) for CsPbBr₃/Cs₄PbBr₆ core/shell NCs were obviously blueshifted compared with CsPbBr3 NCs. As has been demonstrated by Jia, the formation of Cs₄PbBr₆ was formed by further reaction of the surface of CsPbBr₃ NCs, and the shrinking of CsPbBr₃ core after shell coating induced the blue shift of the absorption and PL emission [32]. Meanwhile, PLE spectra of CsPbBr₃ (PL at 510 nm) and CsPbBr₃/ Cs₄PbBr₆ core/shell (PL at 505 nm) NCs were also measured and given in Fig. 1c. To be different with that of CsPbBr₃ NCs, a sharp decrease was observed in the short wavelength region (300-320 nm) for CsPbBr₃/Cs₄PbBr₆ core/shell NCs, which was consistent with the absorption of Cs₄PbBr₆. The formed type I heterostructure had a band structure with Cs₄PbBr₆ (3.96 eV) as the shell layer and CsPbBr₃ (2.45 eV) as the core layer. PLQY of the as-synthesized CsPbBr3 NCs was measured to be 45% (Fig. S1a), in accordance with some previous reports [34]. Unsurprisingly, CsPbBr₃/ Cs₄PbBr₆ core/shell NCs performed a PLQY as high as 87.23% (Fig. S1b), corresponding to an improvement of about 42%. The PL enhancement could be mainly attributed to the effective passivation of surface defects by the Cs₄PbBr₆ shell layer, as well as the reduction of agglomeration for CsPbBr3 NCs.

The stability of CsPbBr₂ NCs was also improved by the core-shell structure. PL intensities over a long period of time were monitored for CsPbBr3 NCs and CsPbBr3/Cs4PbBr6 core/shell NCs in a conventional environment (Fig. 1d). In contrast to CsPbBr₃ NCs, CsPbBr₃/ Cs₄PbBr₆ core/shell NCs exhibited excellent PL stability. As shown in the figure, CsPbBr₃/Cs₄PbBr₆ core/shell NCs could still maintain more than 60% of the PL intensity after 96 h, while the PL for CsPbBr₃ NCs alone almost disappeared. More details about changes in PL and absorption intensity for both samples are shown in Fig. S2. Both the PL and absorption spectra for core/shell NCs showed more robust with the time than those of CsPbBr₃ NCs. The absorption peak at 313 nm and absorption edge at 505 nm for CsPbBr₃/Cs₄PbBr₆ NCs still existed even after 144 h, while the absorption edge at 505 nm for CsPbBr3 NCs almost disappeared after just 72 h. Because of the protection from the oxygen, light irradiation, and especially moisture in normal environment by Cs₄PbBr₆, CsPbBr₃/Cs₄PbBr₆ core/shell NCs exhibited better stability than CsPbBr₃ NCs [29].

XRD characterizations were carried out to examine the crystal structure of CsPbBr3 NCs and CsPbBr3/Cs4PbBr6 core/shell NCs (Fig. 2a). By comparing with the database, the XRD patterns of the sample were in good agreement with the standard XRD patterns, corresponding to PDF cards of 00-018-0364 and 01-073-2478, respectively. To be different with CsPbBr₃ NCs, both the diffraction peaks of CsPbBr₃ and Cs₄PbBr₆ (marked by stars) were observed for CsPbBr₃/Cs₄PbBr₆ core/shell NCs, meaning that both of CsPbBr₃ and Cs₄PbBr₆ existed in the CsPbBr₃/Cs₄PbBr₆ core/shell NCs. In addition, intensities of the diffraction peaks of Cs₄PbBr₆ were much weaker, indicating that the shell layer was thin, TEM, HRTEM and EDX mapping characterizations were performed to identify the morphology and detailed structure of CsPbBr₃ NCs and CsPbBr₃/Cs₄PbBr₆ core/shell NCs. Both of the CsPbBr₃ NCs and CsPbBr₃/Cs₄PbBr₆ core/ shell NCs showed manifest cubic structures with a mean size of approximately 12 nm (Fig. S3). For identifying the morphology and detailed structure of CsPbBr3 and CsPbBr3/Cs4PbBr6 core/shell NCs, the HRTEM images with clear lattice fringes for two samples were given in the insets of Figs. 2b and 2c, respectively. For CsPbBr₃ NCs (Fig. 2b inset), the lattice spacing was measured to be 0.41 nm, which could be well consistent with the (110) plane of CsPbBr₃ crystal. For the core-shell structure, distinct margins with different lattice stripes were observed in the inset of Fig. 2c. The lattice spacing of the shell was measured to be 0.44 nm, which was well consistent with the (113) plane of Cs₄PbBr₆. As for the inner layer, lattice spacing was measured to be 0.58 nm, which could be well consistent with the (100) plane of CsPbBr₃. The HRTEM images of CsPbBr₃/Cs₄PbBr₆ core/shell NCs could confirm the formation of a core-shell structure effectively. The thin shell layer and the formation of core-shell structure did not affect the morphology of CsPbBr₃ NCs. Due to the existence of the shell layer, size of the CsPbBr₃ core layer would reduce resulting in a blue shift of the absorption and emission for CsPbBr₃/Cs₄PbBr₆ core/shell NCs (as given in Fig. 1c). EDX-STEM mapping images of Cs, Pb and Br elements are shown in Fig. S4, and the corresponding atomic proportions of the elements for both samples are shown in Fig. 2d-e. Compared with the ratio 19.6:19.3:61.1 (≈1:1:3) for CsPbBr₃ NCs, the atomic proportions of the elements for CsPbBr₃/Cs₄PbBr₆ core/shell NCs was estimated to be 23.5:18.8:57.7 (between the ratios of 1:1:3 and 4:1:6). Based on the EDX analysis, the respective proportions of CsPbBr₃ and Cs₄PbBr₆ in the core-shell structure was calculated to be 8:1.

Based on the discussions above, CsPbBr₃ NCs and CsPbBr₃/Cs₄PbBr₆ core/shell NCs were fabricated successfully. Here, we would give a brief explanation about the formation process of both samples. According to relevant reports, CsPbBr₃ seeds are generally highly prone to be transformed into Cs₄PbBr₆ NCs in the presence of Cs ions[32,35,36]. Hence, the growth mechanism of CsPbBr₃ NCs and CsPbBr₃ /Cs₄PbBr₆ core/shell NCs can be summarized as below:

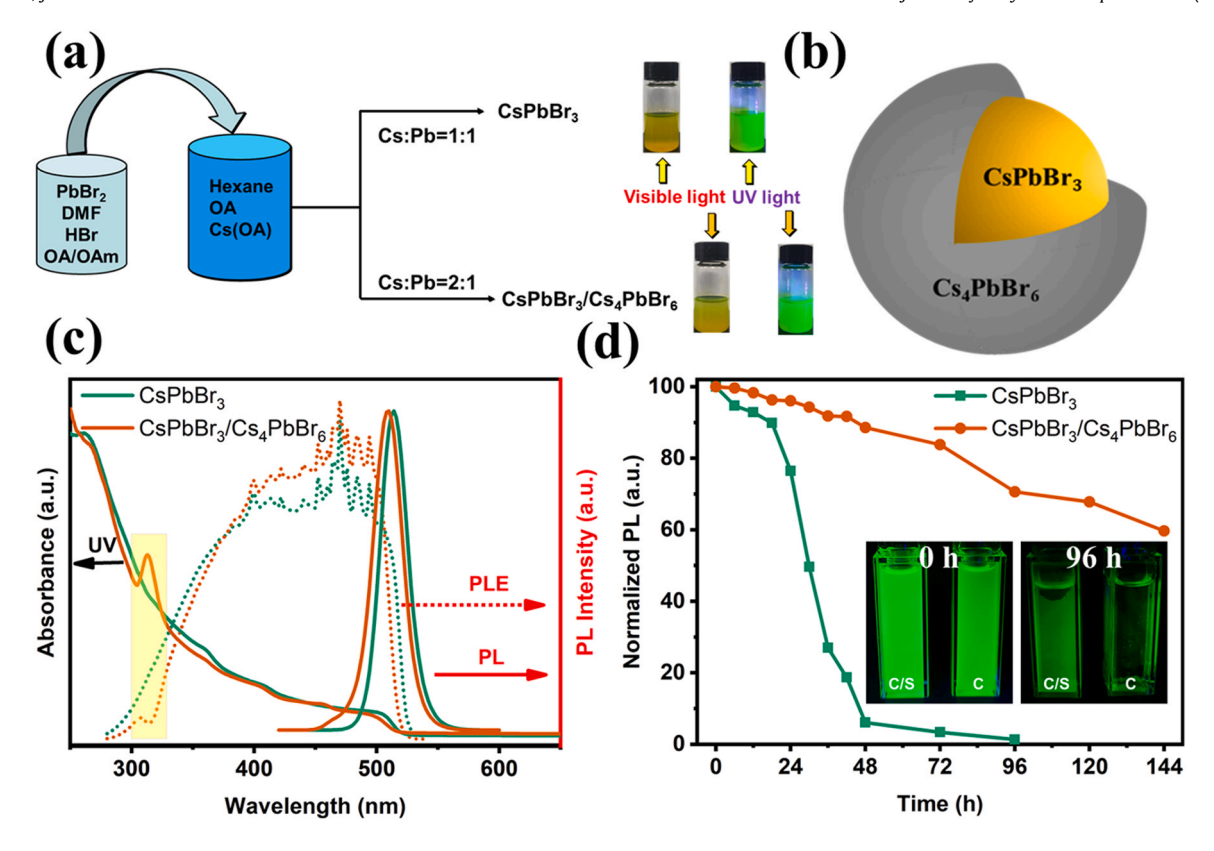


Fig. 1. (a) Schematic of synthesis of CsPbBr₃ NCs and CsPbBr₃/Cs₄PbBr₆ core/shell NCs; (b) 3D schematic diagram of CsPbBr₃/Cs₄PbBr₆ core/shell NCs; (c) Absorption, PL and PLE spectra; (d) Long-term PL stability of CsPbBr₃ NCs and CsPbBr₃/Cs₄PbBr₆ core/shell NCs, the inset is photoluminescence photographs of the samples at 0 h and 96 h (C/S: CsPbBr₃/Cs₄PbBr₆ core/shell NCs, C: CsPbBr₃ NCs).

When the ratio of Cs⁺ to Br⁻ is close to 1:3, the following reaction takes place and CsPbBr₃ NCs are formed:

$$Cs^+ + Pb^{2+} + 3Br^- \rightarrow CsPbBr_3$$

The crystallization process is usually very quick, occurring in a few seconds.

With the increment of Cs⁺ and Br⁻, the above CsPbBr₃ NCs are formed rapidly, and then the surface of CsPbBr₃ NCs would undergo phase transformation to the Cs₄PbBr₆, due to the presence of and excessive Cs⁺ and Br⁻ ions. The specific chemical processes are as follows:

$$Cs^+ + Pb^{2+} + 3Br^- \rightarrow CsPbBr_3$$

$$CsPbBr_3 + 3Cs^+ + 3Br^- \rightarrow Cs_4PbBr_6$$

Considering that the amount of Cs atoms is limited and Cs_4PbBr_6 would acts as an isolation layer to avoid further phase transitions, the thickness of the Cs_4PbBr_6 shell is generally thin, in accordance with the HRTEM images of the Cs_4PbBr_3/Cs_4PbBr_6 core/shell NCs. However, the rate for phase transition could not be precisely controlled, and the morphology and size distributed more widely for Cs_4PbBr_3/Cs_4PbBr_6 core/shell NCs than those of Cs_4PbBr_3 NCs (as shown by Fig. S3).

Beside the passivation effect of the core/shell structure, the formed type I heterostructure would also influence the carrier dynamics of the NCs and enhance the PL property of the sample. Here, time-resolved PL of CsPbBr₃ NCs and CsPbBr₃/Cs₄PbBr₆ core/shell NCs were recorded to explore more photophysical mechanisms, and the results are shown in Fig. 3a. The PL decay process in both CsPbBr₃ and CsPbBr₃/Cs₄PbBr₆ NCs showed a nonlinear decay kinetics, with

an average lifetime of 13.13 ns for CsPbBr₃/Cs₄PbBr₆ and 33.81 ns for CsPbBr₃ NCs. Detailed description of fitting function and related parameters were given in supporting information. The PL lifetime of CsPbBr₃ NCs was longer than that in some previous reports, which could be due to the relatively larger size and lower exciton binding energy [32,37]. Shorter lifetime for CsPbBr₃/Cs₄PbBr₆ may origin from the reduced size of the CsPbBr₃ core and enhanced exciton binding energy. The core may shrink due to ion diffusion after shell formation, which corresponds to the blue shift of the absorption and PL in CsPbBr₃/Cs₄PbBr₆. Temperature-dependent PL in both samples are conducted to measure the exciton binding energy. PL intensity was plotted as a function of temperature and the results were fitted using the following Arrhenius equation [34]:

$$I(T) = I_0/(1 + A \exp(-\frac{E_b}{k_B T}))$$

where I(T) and I_0 are the integrated PL intensities at temperature T and 0 K, respectively. E_b is the exciton binding energy, and k_B is the Boltzmann constant. By fitting the temperature dependent PL results, exciton binding energy for CsPbBr₃/Cs₄PbBr₆ NCs was established to be 200.8 meV (Fig. 3b-c), much larger than that of CsPbBr₃ NCs (92.4 meV) (Fig. 3d-e). Detailed description of fitting function and related parameters were shown in Supporting Information. Hereby, an excitons bandgap model for CsPbBr3 and CsPbBr3 /Cs₄PbBr₆ NCs was proposed as given in Fig. 3f. Due to the lower exciton binding energy, photogenerated carrier would delocalization and widely distribute in the whole nanocrystals for CsPbBr₃ NCs. But for CsPbBr₃/Cs₄PbBr₆ NCs, the shell layer would provide a sufficiently large offset at the conduction and valence band edge due to the larger bandgap for Cs₄PbBr₆ shell, significantly increasing the exciton binding energy of the system and localizing the photogenerated carrier. This type-I bandgap model would not only

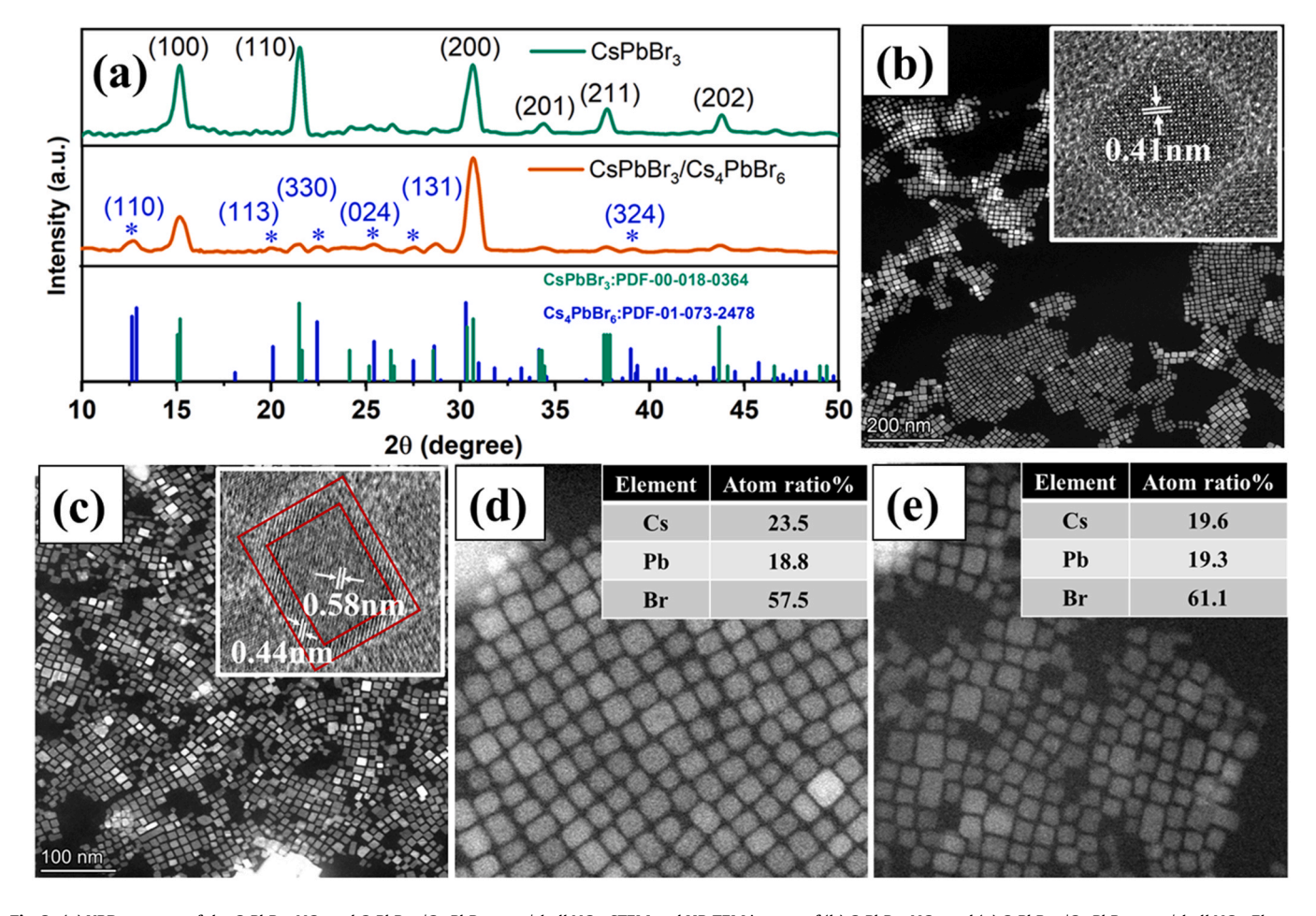


Fig. 2. (a) XRD patterns of the CsPbBr₃ NCs and CsPbBr₃ /Cs₄PbBr₆ core/shell NCs; STEM and HR-TEM images of (b) CsPbBr₃ NCs, and (c) CsPbBr₃ /Cs₄PbBr₆ core/shell NCs; Element atomic distribution of (d) CsPbBr₃ NCs, and (e) CsPbBr₃ /Cs₄PbBr₆ core/shell NCs.

improve the PLQYs, but also can lead to faster decay for CsPbBr₃/Cs₄PbBr₆ core/shell NCs. The confined excitons model was also adopted by other researchers to explain the faster decay for core/shell NCs [38].

To further confirm the confined excitons bandgap model, femtosecond time-resolved transient absorption (TA) measurements were employed to unveil the transfer dynamics of photogenerated carrier in CsPbBr3 and CsPbBr3/Cs4PbBr6 NCs. Here, femtosecond laser with a center wavelength of 400 nm was used as the pump light to excite the carriers. Fig. 4a shows the pseudo-colored TA spectra in CsPbBr₃/Cs₄PbBr₆ NCs, and Fig. 4b shows several representative TA spectra at certain delay time. The results for CsPbBr₃ NCs are given in Fig. S5a-b. From the TA spectra, a negative absorption at 510 nm and a positive absorption band at 475 nm was attributed to ground state bleaching (GSB) and photo induced absorption (PIA) for CsPbBr₃ NCs, respectively [39]. When the CsPbBr₃ NCs was excited, carriers in valence band (VB) were excited to conduction band (CB), causing the filling of CB and bleaching of ground state absorption. The PIA signal was originated from the absorption arising from the excited state carriers. For CsPbBr₃ /Cs₄PbBr₆ core/shell NCs, a negative absorption band at 500 nm was presented. Multiple exponential fitting was used to further handle the time-resolved TA curves for both samples at 510 nm and 500 nm, respectively. The rise time of GSB are 297 fs and 408 fs for CsPbBr₃ NCs and CsPbBr₃/Cs₄PbBr₆ core/shell NCs (Fig. 4c), corresponding to the excited state hot carrier relaxation time. Reduction of GSB corresponds to the carrier relaxation from excited state to the ground state. The lifetime of the excited state carriers for CsPbBr₃ /Cs₄PbBr₆ core/shell NCs was fitted with 1.8 ns, shorter than 2.3 ns for the

CsPbBr₃ NCs (Fig. 4c). Carrier lifetime difference between the two samples could be well matched with TRPL characterization given in Fig. 3a and originated from the reduced size of the CsPbBr₃ core and enhanced exciton binding energy.

Considering that the bandgap of CsPbBr₃ NCs is 2.45 eV (505 nm) and Cs₄PbBr₆ NCs is 3.96 eV (313 nm), only CsPbBr₃ NCs can be excited by 400 nm femtosecond laser. 350 nm (3.54 eV) and 300 nm (4.13 eV) femtosecond laser are used for pumping to reveal the charge transfer of excited state carriers between CsPbBr₃/Cs₄PbBr₆ core/shell NCs, and further monitoring the rising of the GSB. Excited state carrier energy will improve accompanied by the shorter excitation wavelength, and further enhanced the growth time [40] (Fig. 4e). The rising time for CsPbBr₃ NCs increased from 297 fs at 400 nm to 801 fs at 350 nm (Fig. S5c) and 990 fs at 300 nm. But for CsPbBr₃/Cs₄PbBr₆, other than the increased rising time (408 fs at 400 nm to 875 fs at 350 nm (Fig. S5c)), two different processes were monitored in the GSB establishment time for the CsPbBr₃/Cs₄PbBr₆ core/shell NCs prepared in this paper with the pump wavelength at 300 nm, which were 945 fs (33%) and 3.18 ps (67%) (300 nm) (Fig. 4d)). Through the contrast of rising time at different wavelengths, the following carrier transfer and relaxation models in CsPbBr₃/Cs₄PbBr₆ core/shell NCs are summarized. For the wavelength at 400 nm and 350 nm, only CsPbBr₃ can be pumped and the rising time for the GSB corresponding to the excited state hot carrier relaxation (Fig. 5a). As for 300 nm, CsPbBr₃ and Cs₄PbBr₆ can be pumped together and the rising time for the GSB could not only corresponding to the hot carrier relaxation, but also the carrier transfer from the Cs₄PbBr₆ to CsPbBr₃. For the process with the rising time of 945 fs, it can be attributed to the hot carrier relaxation time

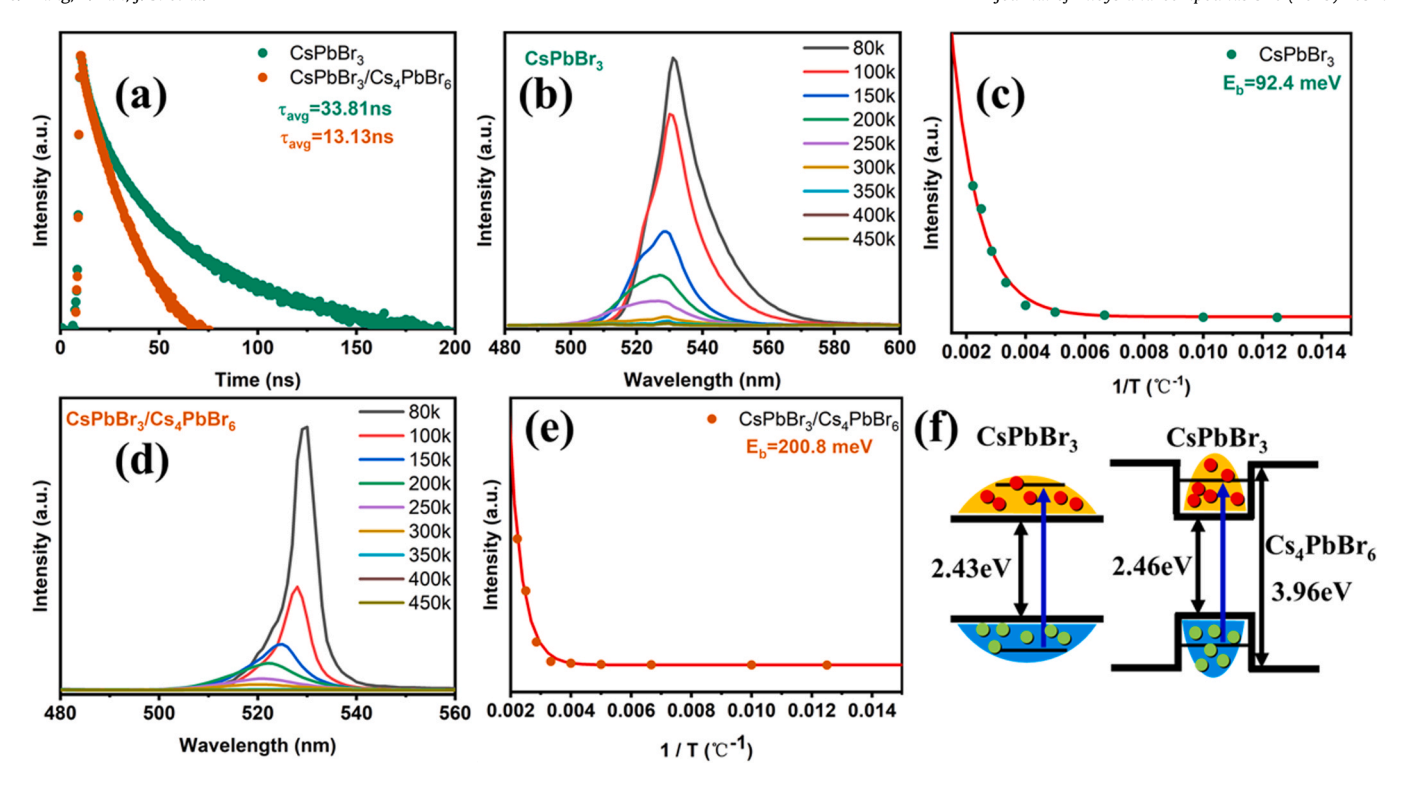


Fig. 3. (a) Time-resolved PL decays of CsPbBr₃ NCs and CsPbBr₃ /Cs₄PbBr₆ core/shell NCs; (b-c) Temperature-dependent PL spectra and integrated PL intensity as a function of temperature of CsPbBr₃ NCs; (d-e) Temperature-dependent PL spectra and integrated PL intensity as a function of temperature of CsPbBr₃ /Cs₄PbBr₆ core/shell NCs; (f) Schematic illustration of the bandgap model for CsPbBr₃ NCs and CsPbBr₃ /Cs₄PbBr₆ core/shell NCs.

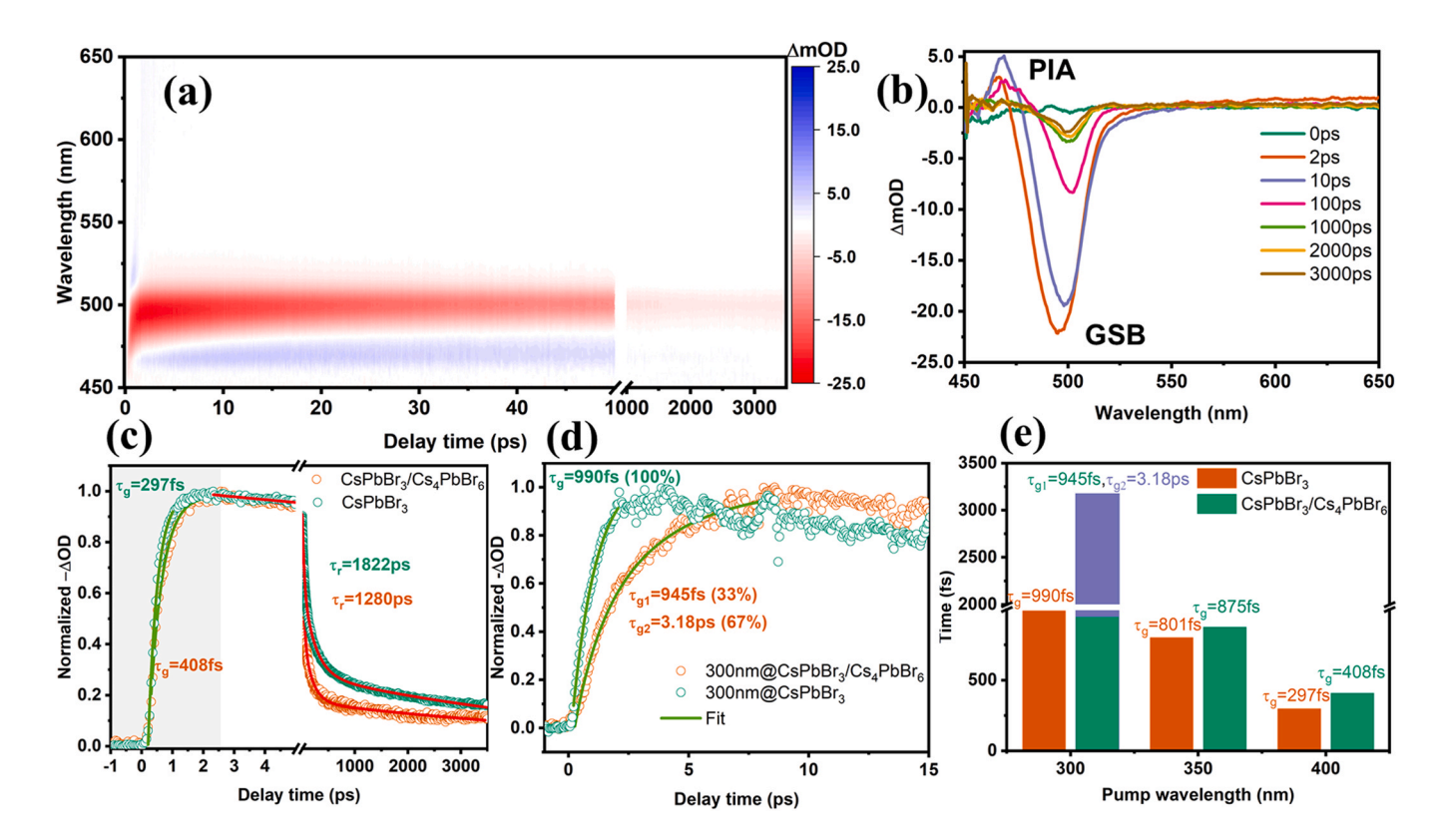


Fig. 4. (a) Representative pseudo-colored, (b) Several representative TA plots of CsPbBr₃ /Cs₄PbBr₆ NCs; (c) Comparative bleaching kinetic traces of CsPbBr₃ and CsPbBr₃ /Cs₄PbBr₆ NCs, respectively; (d) Comparative signal establishment kinetic traces of CsPbBr₃ and CsPbBr₃ /Cs₄PbBr₆ NCs with a pump wavelength at 300 nm; (e) Signal settling time at different pump wavelengths of CsPbBr₃ NCs and CsPbBr₃ /Cs₄PbBr₆ core/shell NCs.

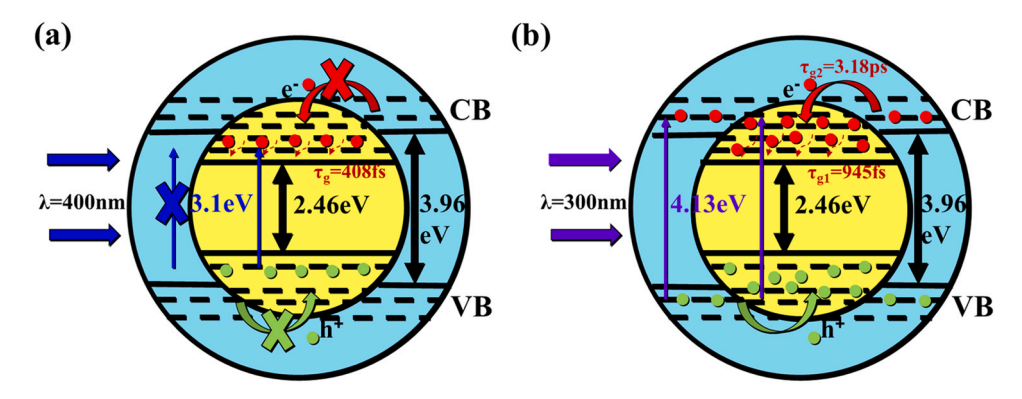


Fig. 5. Schematic of hot carrier relaxation and transfer processes upon (a) 400 nm and (b) 300 nm pump in CsPbBr₃/Cs₄PbBr₆ core/shell NCs.

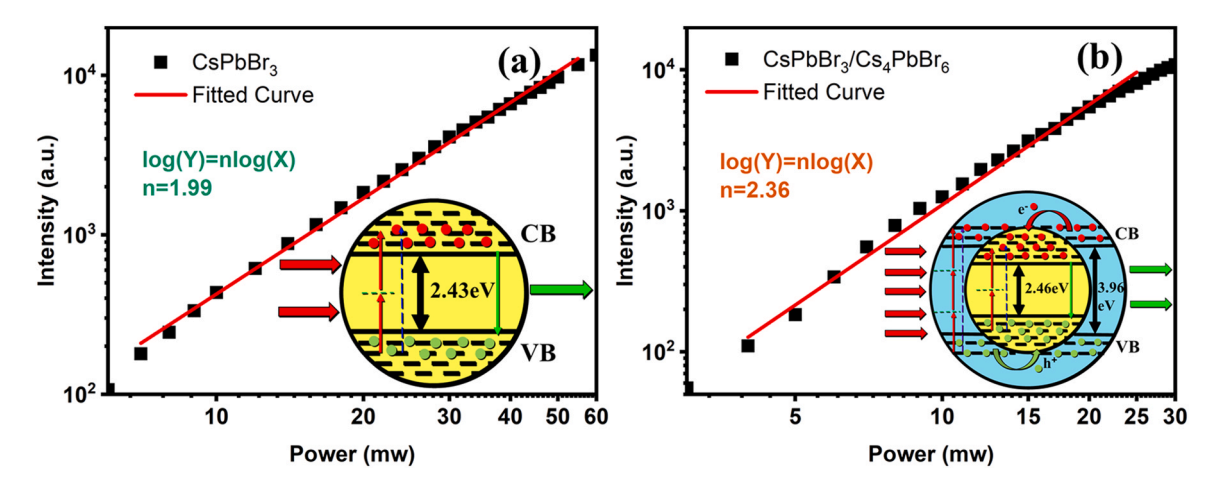


Fig. 6. Two and multiphoton absorption PL and corresponding fitting plots of (a) CsPbBr₃ NCs and (b) CsPbBr₃ /Cs₄PbBr₆ core/shell NCs, respectively. Insets are the corresponding photon absorption and emission schematic diagram, respectively.

contrasting to the time of 990 fs in CsPbBr₃ NCs. While for the longer growth time of 3.18 ps, in combination with confined excitons bandgap model, it was attributed to the carrier transfer from the Cs₄PbBr₆ (Fig. 5b). For the CsPbBr₃/Cs₄PbBr₆ core/shell NCs, excited state carriers of the Cs₄PbBr₆ would be effectively transferred to CsPbBr₃, and would improve the photon utilization efficiency effectively.

To further confirm the bandgap model and energy transfer dynamics in the core/shell NCs, two- or multiphoton PL measurements are conducted [41-44]. Here, femtosecond laser with a central wavelength of 800 nm is used as the excitation. Through changing the intensity of excitation, the PL intensity centered at 525 nm in CsPbBr3 NCs and 505 nm in the core/shell NCs as functions of excitation intensity are recorded. Considering that 800 nm excitation photon energy is 1.5 eV and the bandgap of CsPbBr₃ NCs is 2.46 eV, two photons would be absorbed and then fluorescence through carrier radiative recombination occurred. Employing the logarithmic coordinates, we can see that the slope of CsPbBr3 NCs is 1.99 in Fig. 6a (with detail information in Fig. S6a), indicating the twophoton absorption PL. For CsPbBr₃/Cs₄PbBr₆ core/shell NCs, however, the slope of is estimated to be about 2.36 in Fig. 6b (with detail information in Fig. S6b). This result indicates that, not only CsPbBr₃ core can absorb the excitation light through two-photon absorption, but also the Cs₄PbBr₆ shell with a bandgap of 3.96 eV can absorb through multi-photon absorption. The electron transition from the shell to core can contribute to the PL emission in core/shell NCs. In addition, due to the excellent multi-photon absorption PL of the perovskite NCs, the material can be used in multi-photon PL imaging area, improving the spatial resolution of the microscopic system.

4. Conclusions

In summary, by using a facile inverse microemulsion method, strongly luminescent and highly stable CsPbBr₃/Cs₄PbBr₆ core/shell NCs were prepared. The CsPbBr₃/Cs₄PbBr₆ core/shell NCs presented a photoluminescence quantum yields (PLQYs) of 87.23% and long-term stability. A confined excitons bandgap model was proposed for explaining for the high PLQYs through time-resolved PL, temperature-dependent PL measurements. Combining with transient absorption and multi-photon absorption PL, a charge transfer process from Cs₄PbBr₆ shell layer to CsPbBr₃ core layer is further revealed in CsPbBr₃/Cs₄PbBr₆ core/shell NCs. We believe that this work would contribute to the practical application of perovskites and improve our cognition of the PL mechanism of the perovskite core/shell structures.

CRediT authorship contribution statement

Chenxu Wang: Investigation, Conceptualization, Data curation, Writing – original draft. **Lihe Yan:** Supervision, Writing – review & editing. **Jinhai Si:** Supervision, Resources. **Tianyu Huo:** Resources, Data curation. **Xun Hou:** Supervision, Resources.

Data Availability

Data will be made available on request.

Declaration of Competing Interest

The authors declare that they have no known competing financial interests or personal relationships that could have appeared to influence the work reported in this paper.

Acknowledgments

This work was supported by the National Research and Development Program of China (Grant No. 2019YFA0706402) and the National Natural Science Foundation of China (Grant No. 62027822).

Appendix A. Supporting information

Supplementary data associated with this article can be found in the online version at doi:10.1016/j.jallcom.2023.169272.

References

- [1] L. Protesescu, S. Yakunin, M.I. Bodnarchuk, F. Krieg, R. Caputo, C.H. Hendon, R.X. Yang, A. Walsh, M.V. Kovalenko, Nanocrystals of cesium lead halide perovskites (CsPbX(3), X = Cl, Br, and I): novel optoelectronic materials showing bright emission with wide color gamut, Nano Lett. 15 (2015) 3692–3696.
- [2] Y. Wang, X. Li, J. Song, L. Xiao, H. Zeng, H. Sun, All-inorganic colloidal perovskite quantum dots: a new class of lasing materials with favorable characteristics, Adv. Mater. 27 (2015) 7101–7108.
- [3] P. Ramasamy, D.H. Lim, B. Kim, S.H. Lee, M.S. Lee, J.S. Lee, All-inorganic cesium lead halide perovskite nanocrystals for photodetector applications, Chem. Commun. 52 (2016) 2067–2070.
- [4] A. Swarnkar, A.R. Marshall, E.M. Sanehira, B.D. Chernomordik, D.T. Moore, J.A. Christians, T. Chakrabarti, J.M. Luther, Quantum dot-induced phase stabilization of alpha-CsPbI3 perovskite for high-efficiency photovoltaics, Science 354 (2016) 92–95.
- [5] H. Oga, A. Saeki, Y. Ogomi, S. Hayase, S. Seki, Improved understanding of the electronic and energetic landscapes of perovskite solar cells: high local charge carrier mobility, reduced recombination, and extremely shallow traps, J. Am. Chem. Soc. 136 (2014) 13818–13825.
- [6] Q.A. Akkerman, G. Raino, M.V. Kovalenko, L. Manna, Genesis, challenges and opportunities for colloidal lead halide perovskite nanocrystals, Nat. Mater. 17 (2018) 394–405.
- [7] X. Li, Y. Wu, S. Zhang, B. Cai, Y. Gu, J. Song, H. Zeng, CsPbX3 quantum dots for lighting and displays: room-temperature synthesis, photoluminescence superiorities, underlying origins and white light-emitting diodes, Adv. Funct. Mater. 26 (2016) 2435–2445.
- [8] X. Yuan, X. Hou, J. Li, C. Qu, W. Zhang, J. Zhao, H. Li, Thermal degradation of luminescence in inorganic perovskite CsPbBr3 nanocrystals, Phys. Chem. Chem. Phys. 19 (2017) 8934–8940.
- [9] J. Li, L. Wang, X. Yuan, B. Bo, H. Li, J. Zhao, X. Gao, Ultraviolet light induced degradation of luminescence in CsPbBr3 perovskite nanocrystals, Mater. Res. Bull. 102 (2018) 86–91.
- [10] Y. Zhou, Y. Zhao, Chemical stability and instability of inorganic halide perovskites, Energy Environ. Sci. 12 (2019) 1495–1511.
- [11] L. Wu, Q. Zhong, D. Yang, M. Chen, H. Hu, Q. Pan, H. Liu, M. Cao, Y. Xu, B. Sun, Q. Zhang, Improving the stability and size tunability of cesium lead halide perovskite nanocrystals using trioctylphosphine oxide as the capping ligand, Langmuir 33 (2017) 12689–12696.
- [12] J.N. Yang, Y. Song, J.S. Yao, K.H. Wang, J.J. Wang, B.S. Zhu, M.M. Yao, S.U. Rahman, Y.F. Lan, F.J. Fan, H.B. Yao, Potassium bromide surface passivation on CsPbI3-xBrx nanocrystals for efficient and stable pure red perovskite light-emitting diodes, J. Am. Chem. Soc. 142 (2020) 2956–2967.
- [13] L. Xu, S. Yuan, H. Zeng, J. Song, A comprehensive review of doping in perovskite nanocrystals/quantum dots: evolution of structure, electronics, optics, and light-emitting diodes, Mater. Today Nano 6 (2019).
- [14] Z.J. Yong, S.Q. Guo, J.P. Ma, J.Y. Zhang, Z.Y. Li, Y.M. Chen, B.B. Zhang, Y. Zhou, J. Shu, J.L. Gu, L.R. Zheng, O.M. Bakr, H.T. Sun, Doping-enhanced short-range order of perovskite nanocrystals for near-unity violet luminescence quantum yield, J. Am. Chem. Soc. 140 (2018) 9942–9951.
- [15] W. Lv, L. Li, M. Xu, J. Hong, X. Tang, L. Xu, Y. Wu, R. Zhu, R. Chen, W. Huang, Improving the stability of metal halide perovskite quantum dots by encapsulation, Adv. Mater. 31 (2019) e1900682.
- [16] J. Hou, P. Chen, A. Shukla, A. Krajnc, T. Wang, X. Li, R. Doasa, L.H.G. Tizei, B. Chan, D.N. Johnstone, R. Lin, T.U. Schulli, I. Martens, D. Appadoo, M.S. Ari, Z. Wang, T. Wei, S.C. Lo, M. Lu, S. Li, E.B. Namdas, G. Mali, A.K. Cheetham, S.M. Collins, V. Chen, L. Wang, T.D. Bennett, Liquid-phase sintering of lead halide perovskites and metal-organic framework glasses, Science 374 (2021) 621–625.

- [17] Q. Zhong, M. Cao, H. Hu, D. Yang, M. Chen, P. Li, L. Wu, Q. Zhang, One-pot synthesis of highly stable CsPbBr3@SiO2 core-shell nanoparticles, ACS Nano 12 (2018) 8579–8587.
- [18] A. Loiudice, S. Saris, E. Oveisi, D.T.L. Alexander, R. Buonsanti, CsPbBr3 QD/AlOx inorganic nanocomposites with exceptional stability in water, light, and heat, Angew. Chem. Int Ed. Engl. 56 (2017) 10696–10701.
- [19] V.K. Ravi, R.A. Scheidt, A. Nag, M. Kuno, P.V. Kamat, To exchange or not to exchange. suppressing anion exchange in cesium lead halide perovskites with PbSO4-oleate capping, ACS Energy Lett. 3 (2018) 1049–1055.
- [20] V.K. Ravi, S. Saikia, S. Yadav, V.V. Nawale, A. Nag, CsPbBr3/ZnS core/shell type nanocrystals for enhancing luminescence lifetime and water stability, ACS Energy Lett. 5 (2020) 1794–1796.
- [21] Z.J. Li, E. Hofman, J. Li, A.H. Davis, C.H. Tung, L.Z. Wu, W. Zheng, Photoelectrochemically active and environmentally stable CsPbBr3/TiO2 core/ shell nanocrystals, Adv. Funct. Mater. 28 (2017).
- [22] J. Shi, W. Ge, J. Zhu, M. Saruyama, T. Teranishi, Core-shell CsPbBr3@CdS quantum dots with enhanced stability and photoluminescence quantum yields for optoelectronic devices, ACS Appl. Nano Mater. 3 (2020) 7563–7571.
- [23] X. Tang, J. Yang, S. Li, Z. Liu, Z. Hu, J. Hao, J. Du, Y. Leng, H. Qin, X. Lin, Y. Lin, Y. Tian, M. Zhou, Q. Xiong, Single halide perovskite/semiconductor core/shell quantum dots with ultrastability and nonblinking properties, Adv. Sci. 6 (2019) 1900412.
- [24] M.A. Boles, D. Ling, T. Hyeon, D.V. Talapin, The surface science of nanocrystals, Nat. Mater. 15 (2016) 141–153.
- [25] H. Ding, Y. Shan, J. Wang, Q. Xu, J. Han, M. Jiao, K. Cao, M. Liu, H. Mu, S. Zhang, C. Yang, Revealing photoluminescence mechanisms of single CsPbBr3/Cs4PbBr6 core/shell perovskite nanocrystals, RSC Adv. 11 (2021) 30465–30471.
- [26] Q.A. Akkerman, A.L. Abdelhady, L. Manna, Zero-dimensional cesium lead halides: history, properties, and challenges, J. Phys. Chem. Lett. 9 (2018) 2326–2337.
- [27] Z. Gan, F. Zheng, W. Mao, C. Zhou, W. Chen, U. Bach, P. Tapping, T.W. Kee, J.A. Davis, B. Jia, X. Wen, The optical properties of Cs4PbBr6-CsPbBr3 perovskite composites, Nanoscale 11 (2019) 14676–14683.
- [28] L. Rao, Q. Zhang, B. Sun, M. Wen, J. Zhang, S. Yu, T. Fu, X. Niu, CsPbBr3/Cs4PbBr6 heterostructure solids with high stability and photoluminescence for white light-emitting diodes, J. Alloy. Compd. 919 (2022).
- [29] H. Zhang, Q. Liao, Y. Wu, J. Chen, Q. Gao, H. Fu, Pure zero-dimensional Cs4PbBr6 single crystal rhombohedral microdisks with high luminescence and stability, Phys. Chem. Chem. Phys. 19 (2017) 29092–29098.
- [30] J. Álmutlaq, J. Yin, O.F. Mohammed, O.M. Bakr, The benefit and challenges of zero-dimensional perovskites, J. Phys. Chem. Lett. 9 (2018) 4131–4138.
- [31] W. Ge, J. Shi, Y. Tian, M. Xu, Y. Wu, Y. Li, Core-shell CsPbBr3@Cs4PbBr6 nanocrystals dispersed in thermoplastic polyurethane as writeable heat-resistant fluorescent inks, J. Alloy. Compd. 865 (2021).
- [32] C. Jia, H. Li, X. Meng, H. Li, CsPbX3/Cs4PbX6 core/shell perovskite nanocrystals, Chem. Commun. 54 (2018) 6300–6303.
- [33] Y.M. Chen, Y. Zhou, Q. Zhao, J.Y. Zhang, J.P. Ma, T.T. Xuan, S.Q. Guo, Z.J. Yong, J. Wang, Y. Kuroiwa, C. Moriyoshi, H.T. Sun, Cs4PbBr6/CsPbBr3 perovskite composites with near-unity luminescence quantum yield: large-scale synthesis, luminescence and formation mechanism, and white light-emitting diode application, ACS Appl. Mater. Interfaces 10 (2018) 15905–15912.
- [34] H. Yang, Y. Zhang, J. Pan, J. Yin, O.M. Bakr, O.F. Mohammed, Room-temperature engineering of all-inorganic perovskite nanocrsytals with different dimensionalities, Chem. Mater. 29 (2017) 8978–8982.
- [35] Z. Liu, Y. Bekenstein, X. Ye, S.C. Nguyen, J. Swabeck, D. Zhang, S.T. Lee, P. Yang, W. Ma, A.P. Alivisatos, Ligand mediated transformation of cesium lead bromide perovskite nanocrystals to lead depleted Cs4PbBr6 nanocrystals, J. Am. Chem. Soc. 139 (2017) 5309–5312.
- [36] F. Zheng, B. Yang, P. Cao, X. Qian, J. Zou, A novel bulk phosphor for white LDs: CsPbBr3/Cs4PbBr6 composite quantum dots-embedded borosilicate glass with high PLQY and excellent stability, J. Alloy. Compd. 818 (2020).
- [37] Y. Li, T. Ding, X. Luo, Y. Tian, X. Lu, K. Wu, Synthesis and spectroscopy of monodispersed, quantum-confined FAPbBr3 perovskite nanocrystals, Chem. Mater. 32 (2019) 549–556.
- [38] B. Kang, K. Biswas, Exploring polaronic, excitonic structures and luminescence in Cs4PbBr6/CsPbBr3, J. Phys. Chem. Lett. 9 (2018) 830–836.
- [39] X. Liu, P. Zeng, S. Chen, T.A. Smith, M. Liu, Charge Transfer Dynamics at the Interface of CsPbX3 Perovskite Nanocrystal-Acceptor Complexes: A Femtosecond Transient Absorption Spectroscopy Study, Laser & Photonics Reviews, (2022).
- [40] N. Mondal, A. Samanta, Complete ultrafast charge carrier dynamics in photoexcited all-inorganic perovskite nanocrystals (CsPbX3), Nanoscale 9 (2017) 1878–1885.
- [41] J. Li, Q. Jing, S. Xiao, Y. Gao, Y. Wang, W. Zhang, X.W. Sun, K. Wang, T. He, Spectral dynamics and multiphoton absorption properties of all-inorganic perovskite nanorods, J. Phys. Chem. Lett. 11 (2020) 4817–4825.
- [42] W. Chen, F. Zhang, C. Wang, M. Jia, X. Zhao, Z. Liu, Y. Ge, Y. Zhang, H. Zhang, Nonlinear photonics using low-dimensional metal-halide perovskites: recent advances and future challenges, Adv. Mater. 33 (2021) e2004446.
- [43] F. Zhou, X. Ran, D. Fan, S. Lu, W. Ji, Perovskites: multiphoton absorption and applications, Adv. Opt. Mater. 9 (2021).
- [44] Y. Fu, J. Cao, K. Yamanouchi, H. Xu, Air-laser-based standoff coherent raman spectrometer, Ultrafast Sci. 2022 (2022) 1–9.